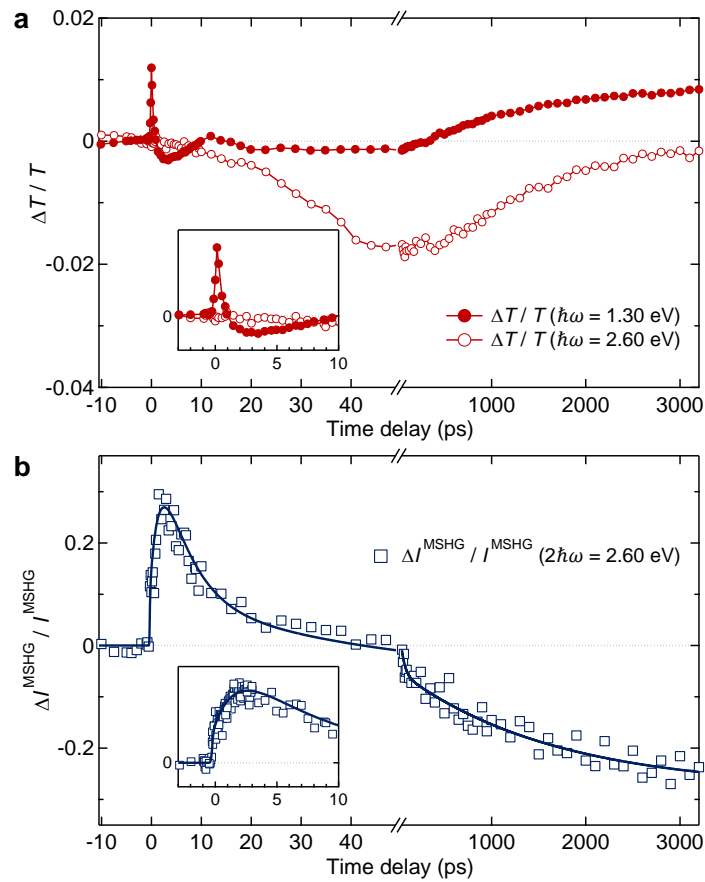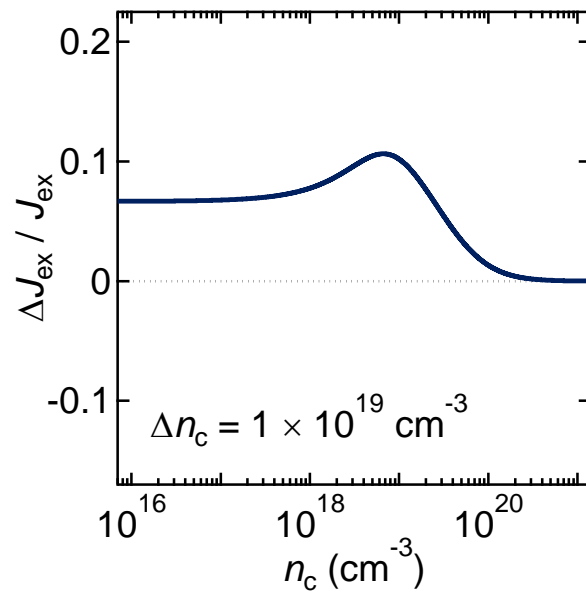# Supplementary Figures



**Supplementary Figure 1 | Comparison between charge dynamics and spin dynamics.**
Time evolution of the change (**a**) of the linear transmittance at the fundamental (1.30 eV) and
the SHG (2.60 eV) photon energy, and (**b**) of the MSHG intensity at 2.60 eV at 77 K for EuO
doped with $x = 2.65\%$ Gd. The excitation density of the pump pulse in (a) and (b) is ~380 $\mu$J cm$^{-2}$.

**Supplementary Figure 2 | Enhancement of $J_{ex}$ alone by the optically increased carrier density.** Modification $\Delta J_{ex}/J_{ex}$ of the exchange coupling by adding a photoinduced carrier density $\Delta n_c = 1 \times 10^{19}$ cm$^{-3}$ to the Gd-dependent carrier density $n_c$ of the conduction band. $\Delta J_{ex}/J_{ex}$ was extracted from Fig. 1a in the main text.

# Supplementary Discussion

## Probing magnetic order by second harmonic generation in EuO

In this section technical details of magnetization-induced optical second harmonic generation (MSHG) in the $Eu_{1-x}Gd_xO$ system are given. This includes a discussion of symmetry and of the coupling to the driving laser fields that implies the relation $I^{MSHG} \propto (J_{ex}M)^2$ for the MSHG process, cf. equation (1) in the main text. We furthermore show that contributions to the MSHG response that are not magnetic in origin but caused by the carrier non-equilibrium distribution after the optical excitation are negligible. Finally, we discuss perturbations from crystallographic, surface and other contributions to the MSHG signal.

**Contributions to the SHG process.** The second harmonic generation (SHG) process can be parameterized by a multipole expansion of the light-matter interaction. In the first two leading orders of this expansion, we get electric dipole (ED) and magnetic dipole (MD) transitions, respectively. We neglect electric quadrupole transitions because experimentally they were identified to be too small to be detected[1-3]. Hence, SHG is described by the relation[4],

$$P_i(2\omega) = \epsilon_0 \left( \chi_{ijk}^{EEE} E_j(\omega)E_k(\omega) + \chi_{ijk}^{EEH} E_j(\omega)H_k(\omega) \right).$$

(1)

Here, the vectors $\mathbf{E}(\omega)$ and $\mathbf{H}(\omega)$ represent the electric- and magnetic-field components of the incident light wave at $\omega$, respectively. $\mathbf{P}(2\omega)$ denotes the nonlinear electric polarization induced at $2\omega$ which acts as source of a light wave of intensity $I \propto |\mathbf{P}(2\omega)|^2$. The nonlinear response tensors $\hat{\chi}^{EEE}$ and $\hat{\chi}^{EEH}$ incorporate the crystal structure and the electronic states and obey the magneto-

crystalline symmetry of the system. $Eu_{1-x}Gd_xO$ possesses the centrosymmetric rock salt structure. This centrosymmetry is retained in the ferromagnetic phase. Even our complete experimental system of (001)-oriented $Eu_{1-x}Gd_xO$ films with perpendicularly incident and emitted light obeys space inversion symmetry within the film plane. Since under this space inversion the incident and emitted fields transform as, $\mathbf{E} \rightarrow -\mathbf{E}$, $\mathbf{H} \rightarrow \mathbf{H}$ and $\mathbf{P} \rightarrow -\mathbf{P}$, the triple-ED SHG response, $\hat{\chi}^{EEE}$, must vanish[5] according to Supplementary Equation (1). Hence, in our $Eu_{1-x}Gd_xO$ system the SHG signal results, in leading multipole order, from one ED and one MD transition in the absorption channel and one ED transition in the emission channel, $\hat{\chi}^{EEH}$. Note that SHG according to $\hat{\chi}^{HEE}$ is suppressed since it does not provide the parity change required for the SHG transition between the $4f$ and the $5d6s$ states depicted in Fig. 1b of the main text.

**Experimental aspects.** For centrosymmetric $Eu_{1-x}Gd_xO$, bulk-generated MD-SHG can more explicitly be written as

$$P_i(2\omega) = \epsilon_0 \left( \chi_{ijk}^{EEH(i)} + \chi_{ijk}^{EEH(c)} \right) E_j(\omega) H_k(\omega). \tag{2}$$

In Supplementary Equation (2), $\hat{\chi}^{EEH(i)}$ and $\hat{\chi}^{EEH(c)}$ denote contributions with linear coupling to, respectively, the paramagnetic crystal or the magnetic order[6,7]. In the (001)-oriented $Eu_{1-x}Gd_xO$ films investigated by us, the non-magnetic SHG contributions according to $\hat{\chi}^{EEH(i)}$ cannot be excited because of symmetry reasons[5]. With the normal-incidence transmission setup sketched in the inset of Fig. 2, the aforementioned surface (non-magnetic) ED-SHG contributions cannot be excited either, since in this geometry the SHG process only involves in-plane components of the light field, which are not sensitive to the inversion symmetry breaking by the surface. Thus, in our experiments, SHG should provide a background-free probe of the magnetic order. This is confirmed by the emergence of the SHG signal at $T_C$. Likewise, the linear dependence of the SHG intensity

on the thickness of the EuO films corroborates that SHG couples to the bulk of the EuO films[1].

Corroborated by theory and experiment (see main text) we furthermore identify an approximated linear dependence of the SHG amplitude on the value of the effective exchange interaction $J_{ex}$.

Microscopically, MSHG in $Eu_{1-x}Gd_xO$ is based on a two-photon transition from the $4f^7$ ground state to the $5d6s$ conduction band[1]. The band state at $2\hbar\omega = 2.60$ eV is resonantly excited and there may be further resonance enhancement by the $4f^65dt_{2g}$ exciton state near $\hbar\omega = 1.30$ eV. This is reminiscent of the doubly resonant MD-SHG process observed in NiO[8].

**Spin dynamics versus electron dynamics.** Measurements, as in Fig. 1c, clearly demonstrate that the SHG process in $Eu_{1-x}Gd_xO$ couples linearly to the magnetic order of the sample. This might, however, no longer be the case when the magnetic state of a sample is investigated in the non-equilibrium state acquired after intense photoexcitation. The redistribution of the charge carriers by the pump pulse and the ensuing relaxation dynamics may also influence the MSHG signal.

In order to scrutinize this issue we performed time-resolved linear transmission measurements on the $Eu_{1-x}Gd_xO$ system. The transmittance (or reflectance) is an established probe for studying charge-carrier dynamics because it directly reproduces the population of the electronic states affected by the pump pulse[9-12]. Supplementary Figures 1a and 1b show transient linear transmittance at the photon energies of the fundamental and the frequency-doubled light in comparison to the time-dependent change of the MSHG signal. The linear transmittance displays a highly complex dynamics that remains to be understood; the theoretical analysis is currently in progress. But even without having completed this analysis, it is already obvious that the dynamics and the amplitude of the transmittance and the MSHG data are substantially different, revealing that the MSHG transient is not noticeably caused by transient

artifacts that are not magnetic in origin[13,14]. We can therefore conclude that the MSHG process truly probes the dynamics of the magnetic order whereas it is not directly perturbed by the charge carrier dynamics.

Another carrier-related contribution to the SHG signal that might be suspected is related to the absorption of the pump light. It leads to an exponential decrease of the pump-light intensity and, hence, of the density of photoexcited carriers across the thickness of the $Eu_{1-x}Gd_xO$ films. The carrier density gradient breaks the inversion symmetry and might lead to additional SHG tensor components. The presence of such contributions in the MSHG signal can, however, be excluded for three reasons. First, its temporal evolution would reflect that of the transmittance at $\omega$. Yet, such SHG contributions were not detected. Second, the absorption of the pump light is so moderate that the related carrier density changes by a factor of less than two across the films investigated by us. Third, carrier gradient contributions to SHG would occur below and above the magnetic ordering temperature. Above $T_C$ the SHG signal in the photoexcited samples is, however, zero at all delays.


## Enhancement of $J_{ex}$ by optically increased carrier density

In the main text we emphasize that for obtaining a photoinduced enhancement or attenuation of the magnetic order it is absolutely essential to consider the combined effects of the photoinduced population of the $5d6s$ conduction band and of the population-dependent shift of the conduction band towards the Gd impurity band. In order to further illustrate this point we calculated how the photoinduced population of the $5d6s$ conduction band alone affects $J_{ex}$. Supplementary Figure 2 shows $\Delta J_{ex}/J_{ex}$ obtained by increasing the equilibrium carrier density $n_c$ of the $5d6s$ band by a

fixed value $\Delta n_c = 1 \times 10^{19}$ cm$^{-3}$ which represents the photo-carrier density in our experiment. The relation between $\Delta J_{ex}$ and $\Delta n_c$ was derived by combining the relation between $T_C$ and $n_c$ in Fig. 1a with the relation between $J_{ex}$ and $T_C$ in ref. 15. Supplementary Figure 2 reveals an increase of $J_{ex}$ up to ~10%. For low values of $n_c$, $\Delta n_c$ simply sets the net carrier density to $10^{19}$ cm$^{-3}$ which results in a constant shift of $\Delta J_{ex}$. For high values of $n_c$ the increase of the net carrier density by $\Delta n_c$ is negligible, and so is $\Delta J_{ex}$. Only for $n_c \approx \Delta n_c$ we observe a pronounced dependence of $\Delta J_{ex}$ on $n_c$. Up to $n_c \approx \Delta n_c$ Supplementary Fig. 2 and Fig. 4a look quite similar. We do, however, never observe a decrease of $J_{ex}$ towards higher values of $n_c$. For explaining this, the aforementioned "dynamic band shift" is essential.

## Theory on the relation between Gd-doping and non-equilibrium RKKY coupling

The RKKY-like magnetic coupling and, hence, the photoinduced enhancement of $J_{ex}$ are proportional to the density of photoexcited non-thermalized conduction electrons which, in turn, is proportional to the conduction electron density of states, $N(\Delta E)$, at the final-state energy of the photoexcited electrons, $\Delta E = \hbar\omega_p - E_{gap}$. As earlier calculations have shown[15], this density of states is sensitively affected by the Gd-doping concentration $x$. Increasing $x$ leads to a downward shift of spectral weight and an enhancement of $N(\Delta E)$ for the photon energy $\hbar\omega_p = 1.55$ eV used in our experiments. We have calculated the RKKY coupling produced by the photoinduced, non-equilibrium electron population in the conduction band, where the latter is renormalized by the presence of the Gd impurities as described above[15]. For $x$ in the order of 1%, this coupling is ferromagnetic and increasing in strength with $x$, whereas, for continued growth of $x$, the ferromagnetic coupling weakens again. In order to extract the effective exchange coupling as

a single number that can be compared with the experiment, first the Curie temperature $T_C$ was calculated for the long-range RKKY coupling using mean-field theory. The effective exchange coupling $\Delta J_{ex}$ (shown in Fig. 4b) was then determined as the effective nearest-neighbor coupling within a Heisenberg model displaying the same value of $T_C$. The interplay of the $x$-dependent increase of density of states and of the weaker ferromagnetic RKKY contributions leads to the non-monotonic behavior of $\Delta J_{ex}/J_{ex}$ depicted in Fig. 4b. Thermalization processes becoming more effective for larger $x$ may lead to an additional reduction of $\Delta J_{ex}$ at $x \gg 1\%$. Note that the theoretical curve of Fig. 4b contains only a single freely adjustable parameter. This is the unknown overlap integral of the conduction electron wave functions with the local $4f$ wave functions. This parameter determines the overall size of $\Delta J_{ex}/J_{ex}$, i.e., the scale on the vertical axis of Fig. 4b. The only other parameter of the model calculation is the ratio of the effective masses of the $5d6s$ conduction electrons and of the heavy holes in the $4f$ band, which was calculated as described in the main text, and is thus not a fit parameter.

# Supplementary References

1.  Matsubara, M., Schmehl, A., Mannhart, J., Schlom, D. G. & Fiebig, M. Large nonlinear magneto-optical effect in the centrosymmetric ferromagnetic semiconductor EuO. *Phys. Rev. B* **81**, 214447 (2010).

2.  Kaminski, *et al*. Spin-induced optical second harmonic generation in the centrosymmetric magnetic semiconductors EuTe and EuSe. *Phys. Rev. Lett.* **103**, 057203 (2009).

3.  Henriques, A. B., Abramof, E. & Rappl, P. H. O. Theory of near-gap second harmonic generation in centrosymmetric magnetic semiconductors: Europium chalcogenides. *Phys. Rev. B* **80**, 245206 (2009).

4.  Pershan, P. S. Nonlinear optical properties of solids: energy considerations. *Phys. Rev.* **130**, 919 (1963).

5.  Birss, R. R. *Symmetry and Magnetism*, (North-Holland, Amsterdam, 1966).

6.  Bennemann, K. H. *Nonlinear Optics in Metals*, (Clarendon Press, Oxford, 1998).

7.  Fiebig, M., Pavlov, V. V. & Pisarev, R. V. Second-harmonic generation as a tool for studying electronic and magnetic structures of crystals: review. *J. Opt. Soc. Am. B* **22**, 96 (2005).

8.  Fiebig, M. *et al*. Second harmonic generation in the centrosymmetric antiferromagnet NiO. *Phys. Rev. Lett.* **87**, 137202 (2001).

9.  Hohlfeld, J., Conrad, U. & Matthias, E. Does femtosecond time-resolved second-harmonic generation probe electron temperatures at surfaces? *Appl. Phys. B: Lasers Opt.* **63**, 541 (1996).

10. Melnikov, A. *et al*. Coherent optical phonons and parametrically coupled magnons induced by femtosecond laser excitation of the Gd(0001) surface. *Phys. Rev. Lett.* **91**, 227403 (2003).

11. Satoh, T., Aken, B. B. V., Duong, N. P., Lottermoser, T. & Fiebig, M. Ultrafast spin and lattice

dynamics in antiferromagnetic $Cr_2O_3$. *Phys. Rev. B* **75**, 155406 (2007).

12. Matsubara, M., Kaneko, Y., He, J.-P., Okamoto, H. & Tokura, Y. Ultrafast polarization and magnetization response of multiferroic $GaFeO_3$ using time-resolved nonlinear optical techniques. *Phys. Rev. B* **79**, 140411(R) (2009).

13. Koopmans, B., van Kampen, M., Kohlhepp, J. T. & de Jonge, W. J. M. Ultrafast magneto-optics in nickel: Magnetism or optics? *Phys. Rev. Lett.* **85**, 844 (2000).

14. Carpene, E. *et al*. Measurement of the magneto-optical response of Fe and $CrO_2$ epitaxial films by pump-probe spectroscopy: Evidence for spin-charge separation. *Phys. Rev. B* **87**, 174437 (2013).

15. Arnold, M. & Kroha, J. Simultaneous ferromagnetic metal-semiconductor transition in electron-doped EuO. *Phys. Rev. Lett.* **100**, 046404 (2008).